PCCP
Physical Chemistry Chemical Physics

Accepted Manuscript

This article can be cited before page numbers have been issued, to do this please use: Y. Chang, J. Zhou, Z. Luo, Z. Chen, Z. He, S. Yu, L. Che, G. Wu, X. Wang, K. Yuan and X. Yang, *Phys. Chem. Chem. Phys.*, 2020, DOI: 10.1039/C9CP05321B.

View Article Online
DOI: 10.1039/C9CP05321B

Revised version for PCCP

Photodissociation Dynamics of H2O and D2O via the D (1A1) Electronic State

Yao Chang[1,2#], Jiami Zhou[2,3#], Zijie Luo[2,4#], Zhichao Chen[2], Zhigang He[2], Shengrui Yu[3], Li Che[4], Guorong Wu[2], Xingan Wang[1*], Kaijun Yuan[2*], Xueming Yang[2]

1. *Department of Chemical Physics, School of Chemistry and Materials Science, University of Science and Technology of China. Jinzhai Road 96, Hefei, Anhui, 230026, P. R. China*
2. *State key Laboratory of Molecular Reaction Dynamics, Dalian Institute of Chemical Physics, Chinese Academy of Sciences, 457 Zhongshan Road, Dalian, 116023, China*
3. *Hangzhou Institute of Advanced Studies, Zhejiang Normal University, 1108 Gengwen Road, Hangzhou, Zhejiang, 311231, P. R. China*
4. *Department of Physics, School of Science, Dalian Maritime University, 1 Linghai Road, Dalian, Liaoning 116026, P. R. China*

#) These authors have equally contributions.

*) To whom correspondence should be addressed. Email address: xawang@ustc.edu.cn, kjyuan@dicp.ac.cn

View Article Online
DOI: 10.1039/C9CP05321B

Abstract

Photodissociation dynamics of H_2O and D_2O via the $\tilde{D}$ state by one-photon excitation have been investigated using the H/D atom Rydberg tagging time-of-flight technique. TOF spectra of the H/D-atom product in both parallel and perpendicular polarizations have been measured. Product translational energy distributions and angular distributions have been derived from TOF spectra. By simulating these distributions, quantum state distributions of the OH/OD product as well as the state-resolved angular anisotropy parameters were determined. The most important pathway of the H_2O/D_2O dissociation via the $\tilde{D}$ state leads to the highly rotationally excited OH/OD(X, v=0) products, while vibrationally excited OH/OD products with $v\geq1$ comprise only one third of the total OH/OD(X) population. The branching ratios of OH(A)/OH(X) and OD(A)/OD(X) have also been determined, 1.0/3.0 for H_2O at 122.12 nm and 1.0/2.2 for D_2O at 121.95 nm, which are reasonably consistent with the values predicted by the previous theory.

View Article Online
DOI: 10.1039/C9CP05321B

I. INTRUDUCTION

The photochemistry of the water molecule has revealed a wealth of quantum phenomena which arise from the involvement of several coupled electronic states with very different potential energy surfaces (PESs). During the last few decades, extensive studies have been performed on this system. [1-3] The absorption spectrum of water below 200 nm presents at least four distinctive regions. [4] Excitation in its longest wavelength ultraviolet absorption band around 150-200 nm leads to the lowest excited singlet state ($\tilde{A}^1B_1$). Dissociation from this state proceeds on a single repulsive PES leading to an H atom and a ground state OH ($X^2\Pi$) product with little internal excitation. [5-13] The second absorption band, corresponding to the $\widetilde{B}\,^1A_1$ state, is centered at 128 nm, with some diffuse progression superimposed on the continuum. The dissociation dynamics from the $\widetilde{B}$ state is fairly intricate due to the complexity of its PES and various nonadiabatic couplings between the $\widetilde{B}$ state and the low-lying states. [14-16] Direct dissociation on this surface leads to an H atom plus the OH partner in the electronically excited state $A^2\Sigma^+$. However, although OH (A) molecules are produced, the dominant pathway leads to an H atom plus a ground state OH (X) molecule via nonadiabatic crossings from the $\widetilde{B}$ state to the PESs of either the $\widetilde{A}$ state or the ground state of water ($\widetilde{X}\,^1A_1$). [17-26] In both cases the OH products are highly rotationally excited, but with limited vibrational excitation. These detailed photodissociation dynamics have been investigated at the Lyman-α wavelength (121.6 nm). [27-34] Yang and coworkers [27, 32] observed striking even-odd intensity oscillations

View Article Online
DOI: 10.1039/C9CP05321B

in the OH(X, v=0) product rotational distribution. These oscillations had been attributed to the dynamical interference between the two conical intersection (CI) pathways.

The $\tilde{C}^1B_1$ state of the water molecule, reached at around 124 nm, is the first Rydberg state with fully resolved rotational structures by one-photon or multi-photon absorptions. [35-39] Two different predissociation mechanisms, which are highly dependent on the K_a rotational excitation, have been revealed from one-photon induced predissociation dynamics studies (For H_2O, an asymmetric top[39], the rotational quantum states are labelled *as* $J_{Ka,Kc}$, where K_a is the projection of the total rotational angular momentum J on the molecular a-axis, which lies in the plane of the molecule perpendicular to the C_2 rotation axis, and K_c on the c-axis, which lies perpendicular to the molecular plane.).[18, 40-45] It was concluded that, for H_2O in the rotational state with K_a=0, the photodissociation process occurs exclusively via the homogeneous nonadiabatic coupling to the $\tilde{A}$ state, leading to rotationally cold and vibrationally hot OH (X) products (Scheme 1). While for H_2O in rotationally excited state with K_a>0, an additional heterogeneous pathway opens through Coriolis-type coupling to the $\tilde{B}$ state, resulting in rotationally hot and vibrationally cold ground state OH (X) and electronically excited OH (A) products.

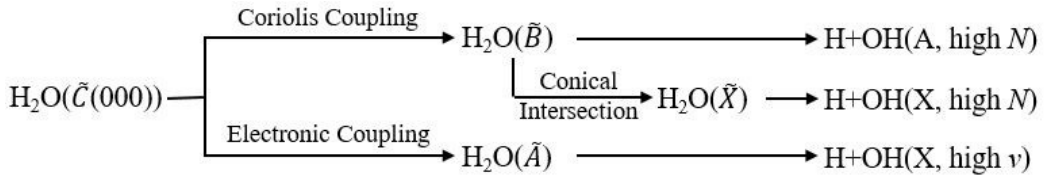

Scheme 1

The $\tilde{D}^1A_1$ state has its electronic origin around 122 nm, and shows no rotational

View Article Online
DOI: 10.1039/C9CP05321B

structure due to the strong coupling with the $\tilde{B}$ state at bent geometry. [25, 46, 47] This strong nonadiabatic coupling leads to a fast homogeneous, purely electronic predissociation. Steinkellner *et al.* [48] reported the lifetime of 60±50 fs for the $\tilde{D}$ state of H_2O using the femtosecond laser pump-probe technique, in accord with the value of 52 fs obtained by He *et al.*[41]. Fillion *et al*. [17] measured the OH (A) fluorescence in the photodissociation of H_2O at 122 nm using synchrotron radiation as a tunable VUV photolysis source. The rotational distribution of the OH (A) product was found to be inverted, with the population peaking at high rotational levels. In that study, however, no ground state OH product information was measured. Therefore, the full state-to-state dynamical picture of the $\tilde{D}$ state dissociation of water has not been obtained thus far experimentally.

On the other hand, previous experimental and theoretical results showed significant discrepancies in the OH(A)/OH(X) branching ratios at 121.6 nm photodissociation of H_2O. Mordaunt *et al.* [33] have reported a branching ratio of 1.0/4.6 by using H-atom Rydberg tagging technique at 121.6 nm photolysis, which was consistent with that reported by Harich *et al.* [27]. However, the theoretical study by van Harrevelt and van Hemert [26] yielded a branching ratio of 1.0/2.5 at 121.6 nm, which was much higher than the measured values. Since the calculated dissociation dynamics were performed on the adiabatic $\tilde{B}$ state surface, they cautioned that electronic states in addition to the $\tilde{B}$ state may be involved at this high photolysis energy. From the absorption spectrum (shown in **Figure 1**), it seems that the tail of the $\tilde{B}$ band can extend to wavelengths shorter than 120 nm, which means both the

View Article Online
DOI: 10.1039/C9CP05321B

$\widetilde{B} \leftarrow \widetilde{X}$ and $\widetilde{D} \leftarrow \widetilde{X}$ transitions are accessible at 121.6 nm. The relative contributions of these two transitions to the absorption at 121.6 nm in molecular beam conditions are, however, difficult to be estimated from the absorption spectrum.

In this paper, we would like to report the results of our recent experimental study on the VUV photodissociation of H_2O at 122.12 nm and D_2O at 121.95 nm (the center of the $\widetilde{D}$ band, marked in Fig. 1), which proceeds predominantly via the $\widetilde{D}$ state, using the H/D-atom Rydberg tagging technique. A state-to-state dynamical picture for the $\widetilde{D}$ state dissociation has been obtained, and compared with the results at 121.6 nm.

II. EXPERIMENTAL METHODS

The experiment methods utilized in this study have been described in details elsewhere [49-53], and only a brief description is presented here. The H/D-atom product in the photolysis region from the photodissociation of H_2O or D_2O in a molecular beam was excited from the ground state to a high Rydberg state via a two-step excitation. In the first excitation step, the H/D atoms were excited to the n = 2 state by a 121.6 nm VUV laser generated by the difference four wave mixing (DFWM) method of 212.5 and 845 nm laser in a Kr gas cell, in which two photons of 212.5 nm are in resonance with the Kr 4p–5p[1/2,0] transition [54]. In the second step, the H/D (n=2) atoms were sequentially excited to a high Rydberg state with n ≈ 50 by a 365 nm laser. The neutral Rydberg H/D atoms, after flying about 74 cm, were then field ionized in front of a micro-channel plate (MCP) detector. The signal received by the MCP was amplified by a fast preamplifier, and counted by a multichannel scaler. The

View Article Online
DOI: 10.1039/C9CP05321B

tunable VUV photolysis source (122.12 nm for H_2O and 121.95 nm for D_2O) was also generated by the DFWM method of 212.5 nm laser (the same as that generating 121.6 nm) with another tunable laser λ_T (~820 nm). The polarization of the photolysis source can be changed by rotating the polarization of the λ_T laser using a waveplate for angular anisotropy measurements. Since the 121.6 nm light also generates H/D atom products from H_2O or D_2O, the 121.6 nm light intensity was decreased by attenuating the 845 nm laser. The 121.6 nm signal was about one magnitude smaller than the tunable VUV photolysis signal and the background subtraction can be achieved easily by alternating the photolysis laser on and off.

III. RESULTS AND DISCUSSIONS

A. Product translational energy distributions

We have measured the H/D-atom time-of-flight (TOF) spectra from H_2O or D_2O photodissociation using the above experimental methods. The photolysis wavelengths chosen in this work lie in the center of the $\tilde{D}$ band, *i.e.*, 122.12 nm for H_2O and 121.95 nm for D_2O. **Figure 2** displays the TOF spectra for H_2O and D_2O with the photolysis laser polarization parallel and perpendicular to the detection axis. The TOF spectrum at the magic angle was also measured to ensure the accuracy of the laser polarization direction. The TOF spectra have been converted to the total translational energy (E_T) distributions using

$$E_T = \frac{1}{2} m_H (1+\frac{m_H}{m_R}) (\frac{d}{t})^2 , \quad (1)$$

where m_H is the mass of the H/D atom, m_R is the mass of the fragment OH/OD, d is the path length from the interaction region to the detector, and t is the flying time of the H/D atom. **Figure 3** and **Figure 4** show the total translational energy

View Article Online
DOI: 10.1039/C9CP05321B

distributions in the two detection directions for H_2O and D_2O, respectively. There are two main groups of clustered peaks in each translational energy spectrum. The group located at the higher translational energy range corresponds to the ground electronic state products OH(X) or OD(X), while the other group in the lower translational energy range corresponds to the electronically excited state products OH(A) or OD(A).

In the molecular photodissociation process, the photodissociation product detected at an angle in the center-of-mass frame (θ_{cm}) relative to the photolysis laser polarization can be represented by the following formula

$$f(E_{T,}\,\theta_{cm}) = \sigma(E_T)\{1 + \beta(E_T)P_2(\cos\theta_{cm})\} \qquad (2)$$

where $\sigma(E_T)$ is the product translational energy distribution, $\beta(E_T)$ is the translational energy dependent anisotropy parameter, $P_2(\cos\theta_{cm})$ is a Legandre polynomial and θ_{cm} is an angle between the recoil direction of the H atom and the photolysis laser polarization in the center-of-mass frame. In this experiment, the translational energy distributions at two photolysis laser polarizations (parallel and perpendicular to the detection axis) were measured, therefore $\sigma(E_T)$ and $\beta(E_T)$ can be calculated.

Because the total energy must be conserved in the dissociation process

$$h\nu + E_{int}(H_2O) = D_o(\text{H-OH}) + E_T(\text{H+OH}) + E_{int}\,(\text{OH}) \qquad (3)$$

where $h\nu$ is the photon energy, and D_o is the dissociation energy. The molecular beam is jet-cooled, so the internal energy of parent molecular H_2O is negligible ($E_{int}(H_2O)$=~0). All sharp peaks observed in the translational energy distributions then can be assigned to the quantum states of the OH (X/A, v, N) or OD (X/A, v, N)

View Article Online
DOI: 10.1039/C9CP05321B

products. Simulations of the product translational energy distributions in the two polarizations have been made using the term values of all rovibrational quantum levels of both the X and A states of the OH and OD product.[27] The Gaussian profiles were used to fit each OH rotational quantum state population, and the linewidth of each profile was assumed to be about 1% of the corresponding translational energy according to the energy resolution. Through tuning the population of each OH quantum state, the summed simulation distribution agrees well with the experimental distribution, as shown in the Figure 3 and 4.

B. OH quantum state distributions and angular distributions

OH quantum state distributions have been determined from simulations of the product translational energy distributions. In total, 11 vibrational states of OH have been included in the fitting of the translational distributions. From the simulations, the dominant dissociation pathway leads to the OH ground electronic state products in the v=0 state, as has been noted in the 121.6 nm photodissociation of H_2O. [27] **Figure 5(a)** displays the rotational distributions of the OH(X, v = 0) products. It is apparent that the OH(X, v = 0) products are extremely rotationally excited with the peak around N = 43, corresponding to about 73% of the available energy depositing into purely rotational excitation, which is similar to that observed at 121.6 nm photodissociation.[27] Such high rotational excitation of the OH product should be due to the dissociation through the CIs at the collinear geometries (HOH and OHH) between the $\tilde{B}$ and $\tilde{X}$ surfaces, following the fast internal conversion from the initial excited $\tilde{D}$ state to the $\tilde{B}$ state. A clear oscillation[32] of the rotational

View Article Online
DOI: 10.1039/C9CP05321B

distribution is also observed around N=40, which has been attributed to quantum interferences between the two $\widetilde{B}$ - $\widetilde{X}$ CI pathways. The fluctuation is more severe than that observed at 121.6 nm, suggesting the quantum interferences are sensitive to the excitation energy.

The vibrational distribution has also been obtained by integrating the rotational distributions for each vibrational level. **Figure 6 (a)** shows the vibrational distribution of the OH (X) products at 122.12 nm. It is clear that the OH(X, v=0) product is the most important single vibrational product channel, while vibrationally excited OH products with v≥1 comprise approximately one third of the total OH(X) population. The vibrational excitation of the OH(X) products is less obvious than that observed at 121.6 nm photodissociation, in which one half of the total OH(X) products were vibrationally excited.[27] According to the dynamical calculations[27], the extremely rotationally excited OH(X) products from H_2O photodissociation are mainly due to the direct dissociation following a $B \rightarrow X$ inelastic transition at the first CI with a collinear HOH configuration, which involves very modest elongation of the shorter O–H bond and leads predominantly to OH(X, v = 0) product. While the molecules dissociating through the $B \rightarrow X$ transition at the second CI near a collinear OHH configuration are subject to the intramolecular vibrational redistribution, resulting in a more randomized vibrational distribution of the OH(X) product. This means the initial excitation to the $\widetilde{D}$ state at 122.12 nm may cause less dissociative flux propagating towards the OHH CI pathway.

The OH (A) products have also been observed from the H_2O photodissociation on

View Article Online
DOI: 10.1039/C9CP05321B

the $\tilde{D}$ state. **Figure 7** shows the rotational state distributions of the OH (A) product in v=0-2. The OH (A, v = 3) product is not populated for the 122.12 nm photolysis due to the energy threshold. The OH (A, v=0, 1) products are highly rotationally excited, with the population peak of N=20 and 16, respectively. While the rotational distribution of OH (A, v=2) is modest with strong fluctuation. **Figure 6 (b)** displays the vibrational distribution of the OH (A) products. The population of the OH (A) product decreases almost linearly as the vibrational energy increases, which is quite similar to that observed at 121.6 nm photolysis.[27] Since the OH (A) products come from the direct dissociation on the $\tilde{B}$ state surface, the dynamical behavior is dominant by the topology of the $\tilde{B}$ state PES. Thus, it is reasonable that the initial excitation at 122.12 nm and 121.6 nm have similar dynamical effect on the OH (A) product channel.

The distributions of the angular anisotropy parameter have also been determined for the various quantum levels of the OH products. **Figure 5(b)** displays the rotationally dependent anisotropy parameter $\beta(N)$ distributions of the OH(X, v = 0) product. This distribution shows a marked variation in the β parameter over the whole rotational range, indicating probably more than one mechanism involved in the photodissociation process. At lower rotational levels, the value of β fluctuates with N, being moderately positive at N < 18, approaching to zero and becoming moderately negative as N increases. At higher rotational levels (N > 38), β value turns positive again and have a peak value at extremely high rotational quantum number. The total trend is similar to that reported at 121.6 nm photolysis, yet subtle difference is

View Article Online
DOI: 10.1039/C9CP05321B

observed. **Figure 8** shows the rotational state specific anisotropy parameter $\beta(N)$ distributions of the OH(A, v = 0-2) products respectively. The variations in β are quite different from each other. There are also some general features for these distributions. Near the energetic limit, the anisotropy parameter is normally positive with higher values. This probably arises because the generation of high N products requires the experience of large angular forces during the dissociation.

C. OD quantum state distributions and angular distributions

Similar to H_2O, OD quantum state distributions were also determined from the photodissociation of D_2O at 121.95 nm. **Figure 9(a)** shows the rotational distributions for the OD(X, v = 0) products, which is also found to be the dominant ground state vibrational pathway. These products are extremely rotationally excited with a peak at around N=59, corresponding to about 72% of available energy depositing into purely rotational excitation, similar to that observed in the 121.6 nm photolysis of D_2O. [29] There is also an oscillation between N = 56 and N = 62 in this distribution, with odd N having enhanced population with respect to neighboring even N, very similar to that at 121.6 nm photolysis. However, the fluctuation is less obvious than that at 121.6 nm, indicating the dynamical interference of outgoing waves crossing from the two CIs becomes weaker. In the photodissociation of D_2O at 121.6 nm, there are also some smaller oscillations in the rotational distribution at low N values, but less regular than those for H_2O, which had been ascribed to the interferences between the two dynamical pathways $\widetilde{B} \rightarrow \widetilde{A}$ electronic Coriolis (Renner–Teller) coupling at a range of HOH or OHH geometries.[29] However, this oscillation was more obscure in the

View Article Online
DOI: 10.1039/C9CP05321B

photodissociation of D_2O at 121.95 nm, indicating such detailed dynamics are both isotope dependent and excitation energy dependent.

Figure 6 (c) displays the vibrational distribution of the OD (X) products at 121.95 nm. Similar to H_2O, The OD(X, v=0) product is the most important single vibrational product channel, with the fraction value of ~0.75. This is much larger than that obtained at 121.6 nm photodissociation of D_2O.[29] Thus, it seems that the initial excitation to the $\tilde{D}$ state of D_2O at 121.95 nm may also cause less dissociative flux propagating towards the ODD CI pathway.

Figure 10 shows the rotational state distributions of the OH (A) product in v=0-3. The OD (A, v=0, 1) products are highly rotationally excited, while the rotational distribution of OD (A, v=2) is modest, and that of OD (A, v=3) is a little colder because of the less available energy obviously. **Figure 6 (d)** displays the vibrational distribution of the OD (A) products. The population of the OD (A) product decreases linearly as the vibrational energy increases, as in H_2O.

Figure 9 (b) shows the rotational state dependent anisotropy parameters for the OD (X, v = 0) product. The values vary strongly over the whole rotational range, rising and falling several times from low N to high N. The total trend is also similar to that at 121.6 nm photolysis. The rotational state dependent anisotropy parameters for the OD (A, v = 0-3) product have been shown in **figure 11**, all of which have the highest anisotropy for rotational states close to the energetic limit. However, there is no clear pattern to these distributions. More detailed theoretical investigations are needed in order to understand fully these detailed dynamical observations.

View Article Online
DOI: 10.1039/C9CP05321B

D. Branching ratios

The branching ratios of the dissociation channels can illustrate the relative importance of the different nonadiabatic dissociation pathways, and are sensitive to the shape of the PES, thus they can serve as an effective probe to the excited surface involved in the couplings with lower PESs. Through careful simulations to the experimental results in this work, the branching ratios of OH(A)/OH(X) and OD(A)/OD(X) have been obtained for H_2O and D_2O. As shown in Table 1, the ratio is 1.0/3.0 for H_2O at 122.12 nm, and 1.0/2.2 for D_2O at 121.95 nm, both are larger than that obtained at 121.6 nm, respectively. The theoretical studies by van Harrelvelt and van Hemert[26] predicted the branching ratios of about 1.0/2.5 for H_2O and 1.0/2.4 for D_2O around 122 nm, which are in reasonable agreement with the experimental values obtained here (Considering the overall error bar of the populations for OH/OD (A) and OH/OD (X) from simulations being about ±20%). Since the calculated dissociation dynamics were just performed on the adiabatic $\tilde{B}$ state surface, such consistence suggests that the dissociation dynamics on the $\tilde{D}$ state can be generally described by using the $\tilde{B}$ state dissociation dynamics. This is reasonable that an avoided crossing between the $\tilde{B}$ and $\tilde{D}$ states locating at the bond angle of about 100° (close to the Frank-Condon region with a bond angle of 104°) [20, 26] , leads to an extremely fast electronically nonadiabatic conversion from the $\tilde{D}$ states to the $\tilde{B}$ state, and the main dynamical features observed eventually are shaped up by the topography of the $\tilde{B}$ state PES. The qualitative similarity of the quantum state distributions and angular distributions observed in this work and that reported at 121.6 nm[27, 29] or other wavelengths at the $\tilde{B}$ state[18] confirms this conclusion. However, some significant differences have also been observed. For example, the branching

View Article Online
DOI: 10.1039/C9CP05321B

ratios between 122.12 or 121.95 nm and 121.6 nm are quite different, which may be due to different excitation energy, since the branching ratios are sensitive to the excitation energy. Previous experimental results showed that the branching ratios of OH(A)/OH(X) increases as the excitation energy increases, from ~1.0/10 at 133.17 nm to ~1.0/5.0 at 128.12 nm, following direct excitation to the $\tilde{B}$ state.[18] However, the branching ratios fluctuate between 1.0/5.0 and 1.0/3.0 when exciting H_2O to the $\tilde{C}$ state[40] or the $\tilde{C}(010)$ state[45], both of which need to undergo an nonadiabatic transition from $\tilde{C} \rightarrow \tilde{B}$ or $\tilde{C}(010) \rightarrow \tilde{D} \rightarrow \tilde{B}$. The coupling strengths between these PESs may be different, however no general trend has been observed. This suggests the CI couplings between the $\tilde{B}/\tilde{X}$ state surfaces and the complicated dynamical nature of the $\tilde{B}$ state PES govern the branching ratios, as noted by the theoretical works.[25] Nonetheless, The state-to-state dynamical pictures shown in this work provide a rigorous test of the PES of the water and the nonadiabatic couplings between these PESs.

IV. CONCLUSIONS

In this study, photodissociation dynamics of H_2O and D_2O on the $\tilde{D}$ state have been investigated using the H/D-atom Rydberg tagging TOF technique combined with a tunable VUV photolysis light source. The quantum state distributions and angular distributions have been determined from the measured TOF spectra, which are similar to that from the 121.6 nm, suggesting that the dissociation from the $\tilde{D}$ state actually dissociates through the $\tilde{B}$ state potential surface via an avoided crossing at bent geometry. The vibrationally excited OH/OD(X) products in this work are much

View Article Online
DOI: 10.1039/C9CP05321B

smaller than that at 121.6 nm, indicating that less dissociative flux propagates toward the OHH(ODD) CI pathway. The dissociation branching ratios of OH(A)/OH(X) and OD(A)/OD(X) have also been obtained, which are 1.0/3.0 for H_2O at 122.12 nm and 1.0/2.2 for D_2O at 121.95 nm.

ACKNOWLEDGEMENTS

The experimental work is supported by the Strategic Priority Research Program of the Chinese Academy of Sciences (Grant No. XDB17000000), the National Natural Science Foundation of China (NSFC Center for Chemical Dynamics (grant no. 21688102)), the National Natural Science Foundation of China (NSFC Nos. 21673232, 21873099, 21922306), and the international partnership program of Chinese Academy of Sciences (No. 121421KYSB20170012). Li Che is supported by National Natural Science Foundation of China (NSFC Nos. 21973010).

Table 1 A comparison of the branching ratios between product channels for photodissociation of H_2O at 122.12 and 121.6 nm, and that of D_2O at 121.95 and 121.6 nm.

	H_2O		D_2O	
Product channels	122.12 nm	121.6 nm[a)]	121.95 nm	121.6 nm[b)]
OD/OH(X)+D/H	3.0	5.1	2.2	3.9
OD/OH(A)+D/H	1.0	1.0	1.0	1.0

a) The data is from Ref.27; b) the data is from Ref.29.

View Article Online
DOI: 10.1039/C9CP05321B

Figures and Captions

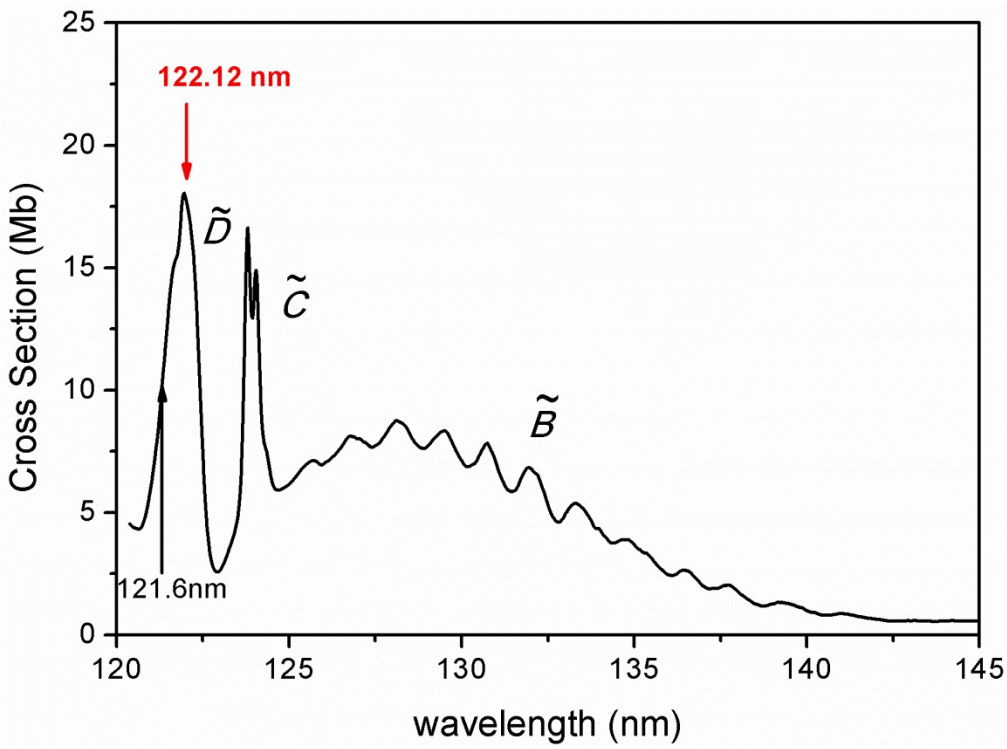

Figure 1 Absorption spectrum of H_2O at room temperature (Adapted from Refs 1). The positions of the photolysis excitation wavelengths used in this work are indicated by downward pointing arrows ($1Mb=1\times10^{-18}cm^2$).

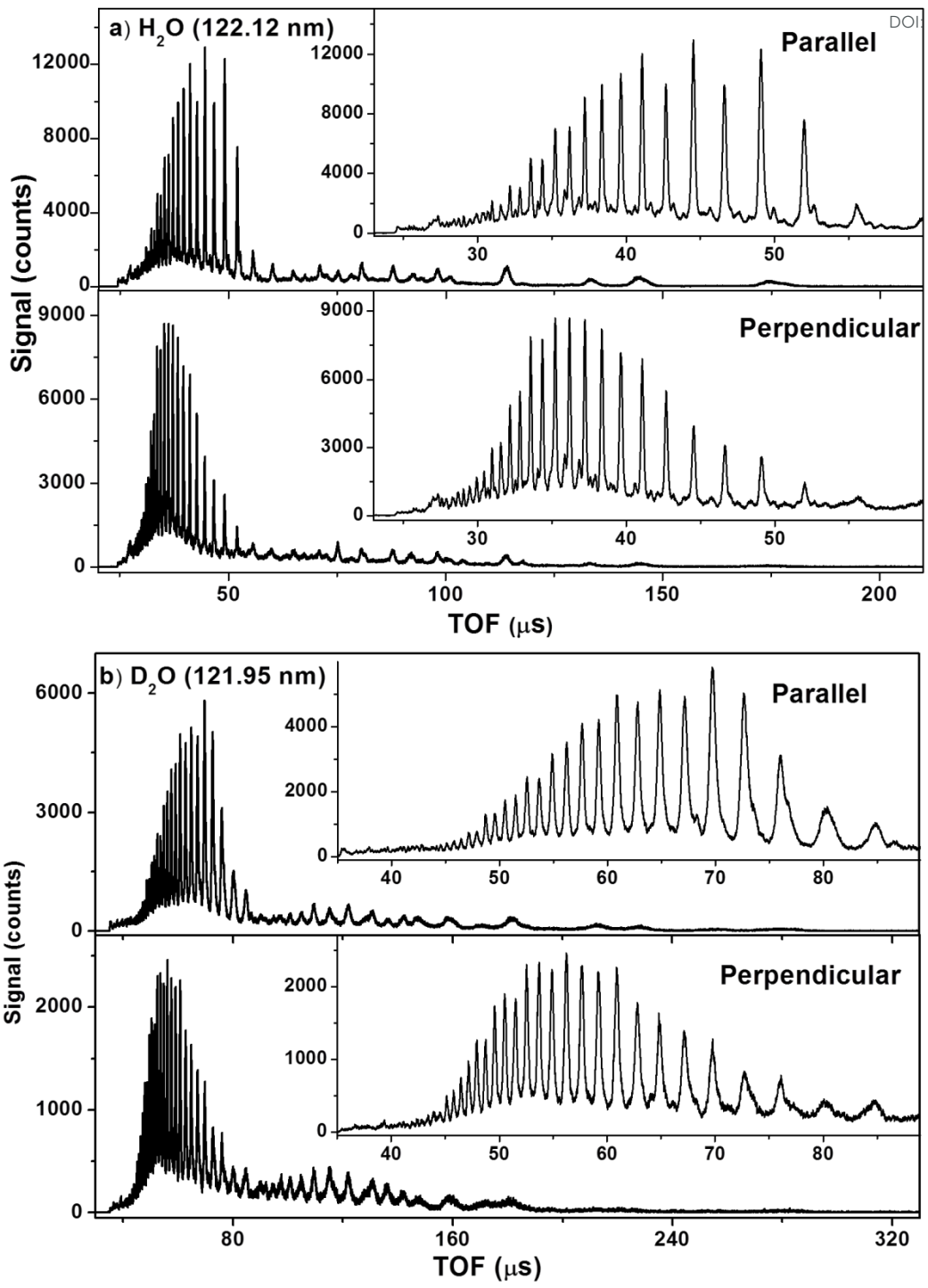

Figure 2. Time-of-flight spectra of the H atom product from the photodissociation of H_2O at 122.12 nm (a) and the D atom product from the photodissociation of D_2O at 121.95 nm (b) with the detection axis parallel and perpendicular to photolysis laser polarization.

View Article Online
DOI: 10.1039/C9CP05321B

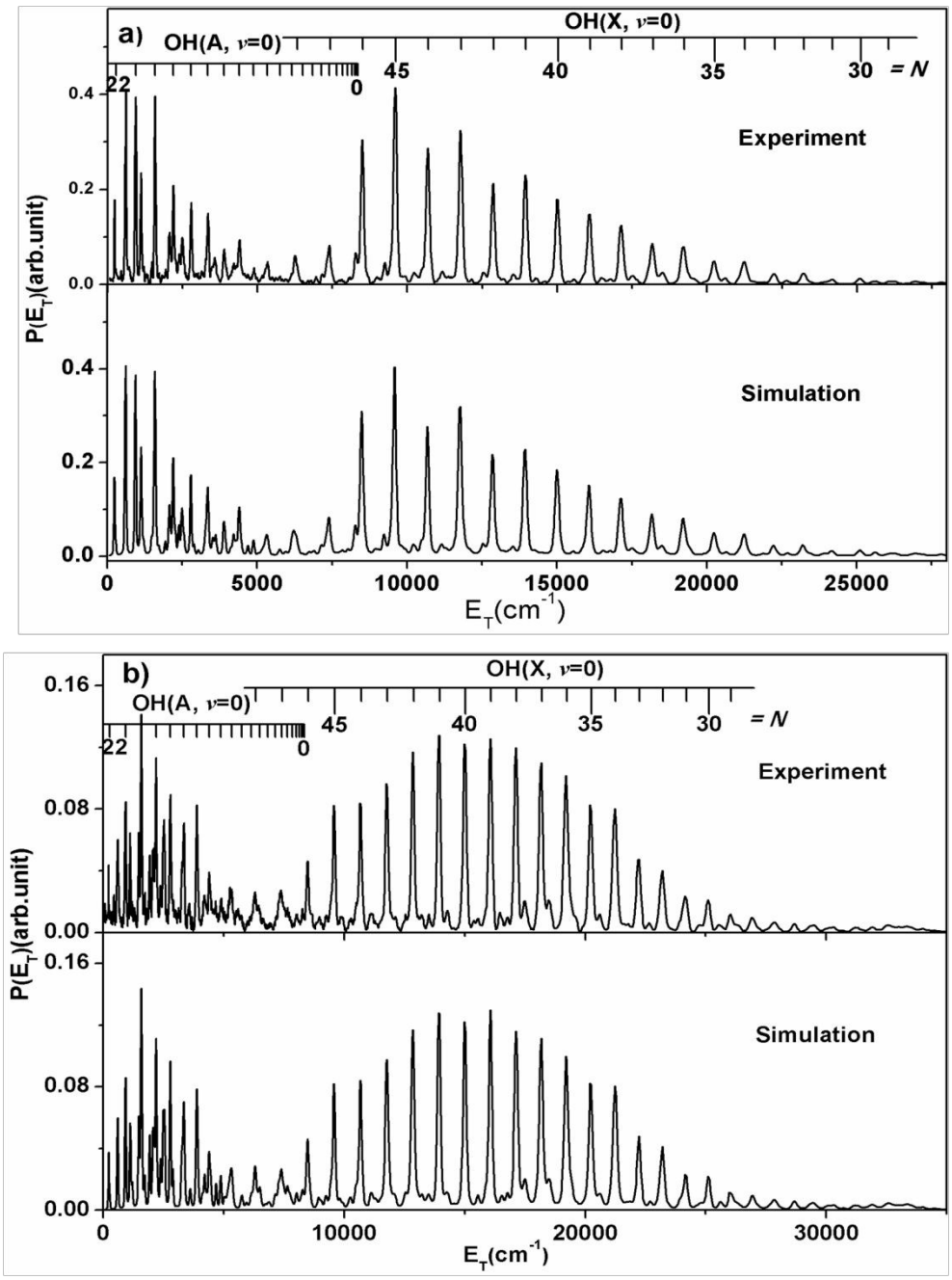

Figure 3. The experimental and simulated product translational energy distributions for the photodissociation of H_2O at 122.12 nm with the detection axis parallel (a) and perpendicular (b) to photolysis laser polarization.

View Article Online
DOI: 10.1039/C9CP05321B

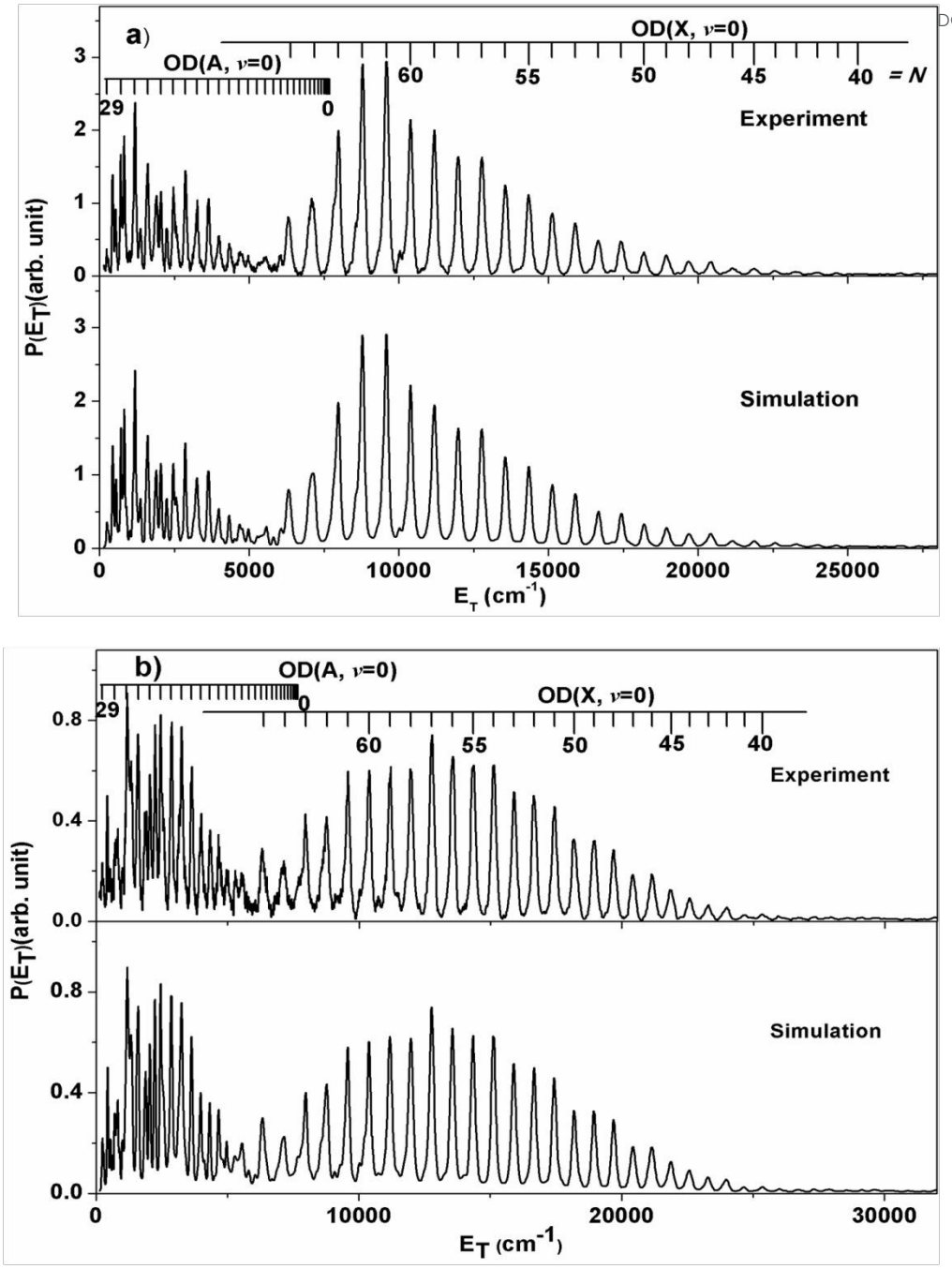

Figure 4. The experimental and simulated product translational energy distributions for the photodissociation of D_2O at 121.95 nm with the detection axis parallel (a) and perpendicular (b) to photolysis laser polarization.

View Article Online
DOI: 10.1039/C9CP05321B

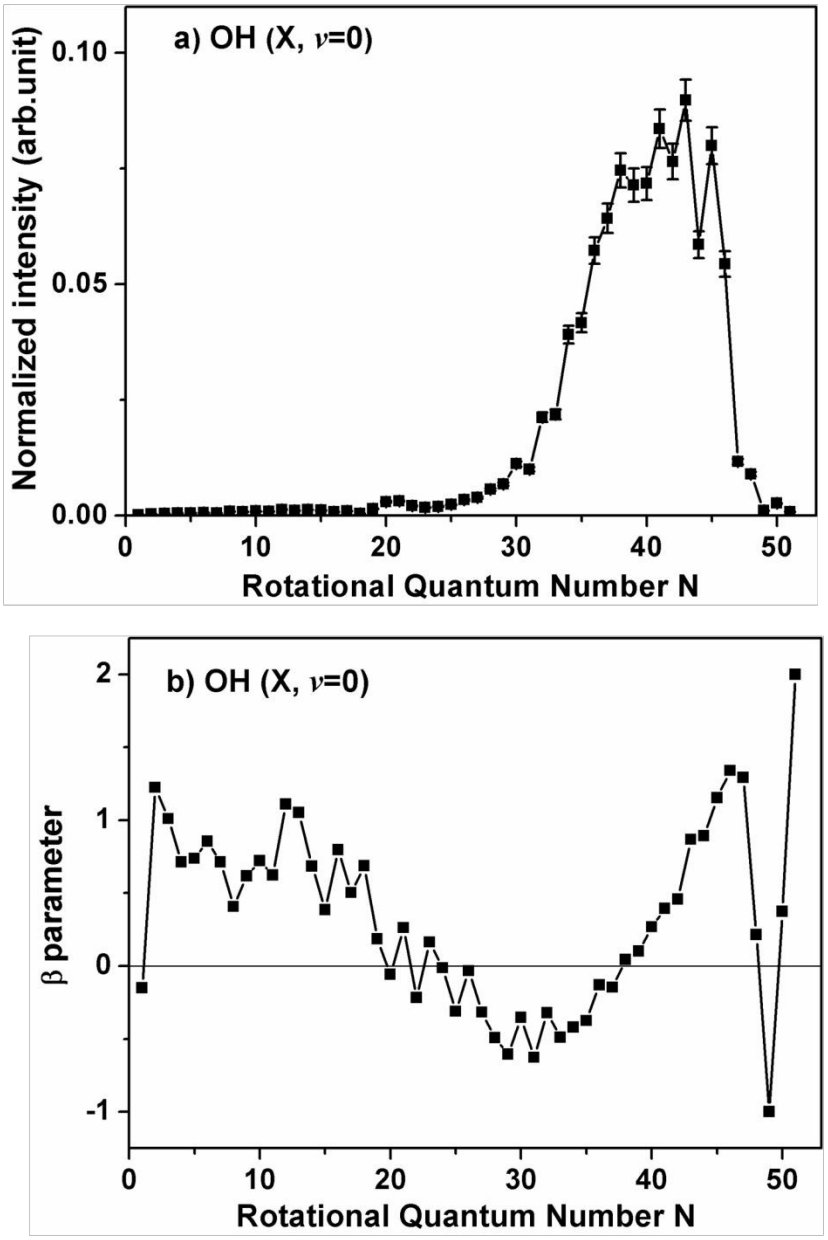

Figure 5. (a) Rotational state distributions of the OH (X, v = 0) products from the photodissociation of H_2O at 122.12 nm and (b) rotational dependence of the anisotropy β for the OH (X, v = 0) products.

View Article Online
DOI: 10.1039/C9CP05321B

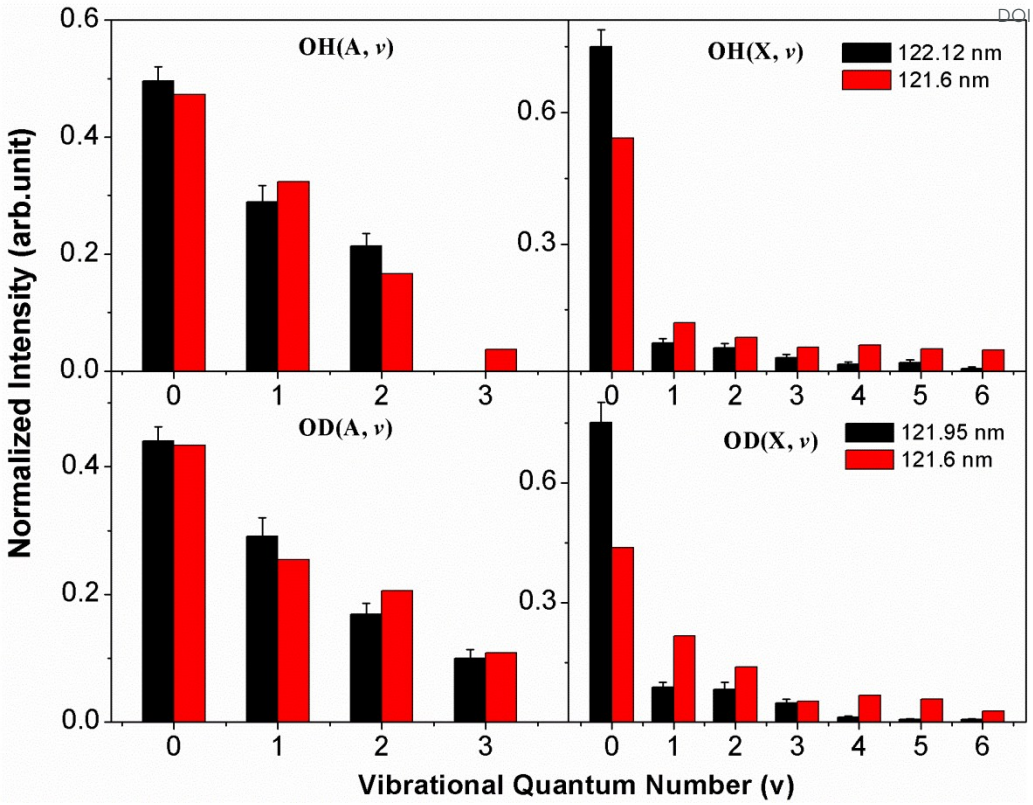

Figure 6. Vibrational state distributions of the OH (X) and OH (A) products from the photodissociation of H_2O at 122.12 nm, and that of the OD (X) and OD (A) products from the photodissociation of D_2O at 121.95 nm. The data of 121.6 nm is adapted from Ref.27.

View Article Online
DOI: 10.1039/C9CP05321B

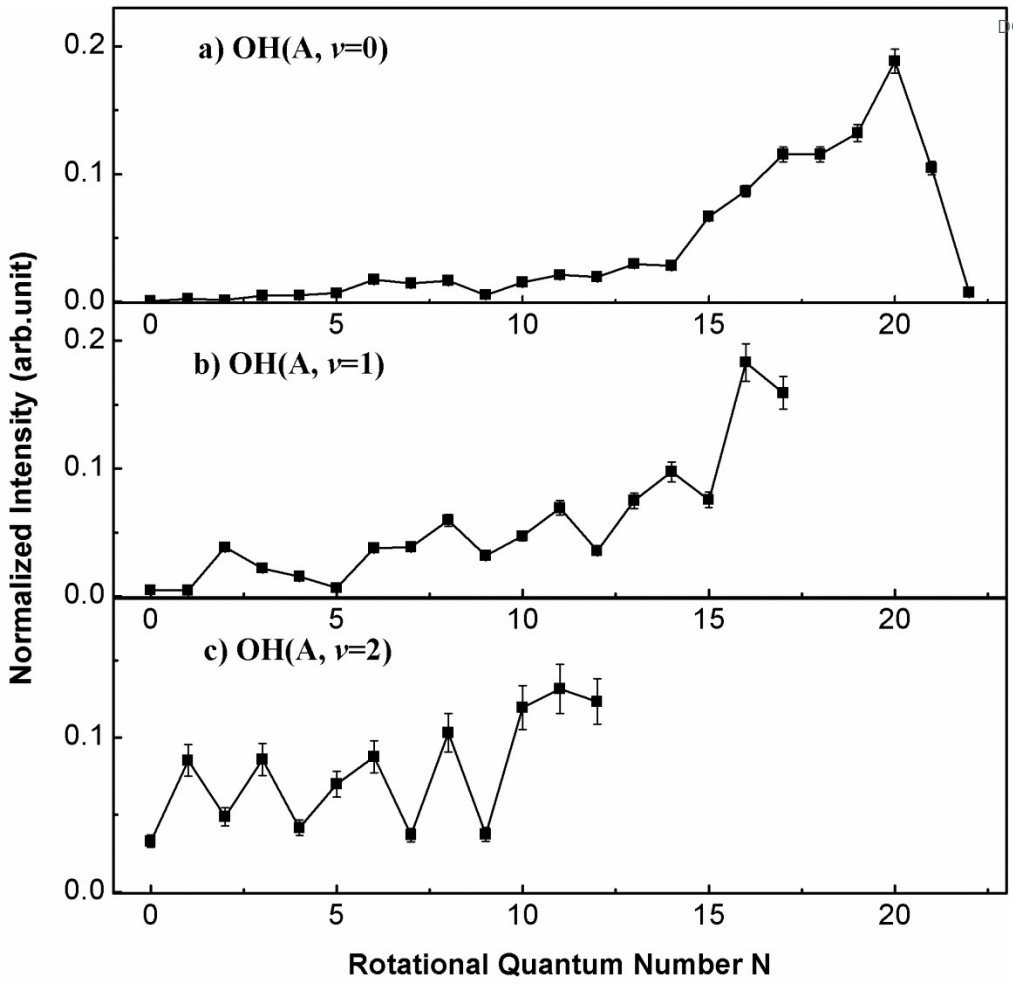

Figure 7. Rotational state distributions of the OH (A, v = 0, 1, 2) products from the photodissociation of H_2O at 122.12 nm.

View Article Online
DOI: 10.1039/C9CP05321B

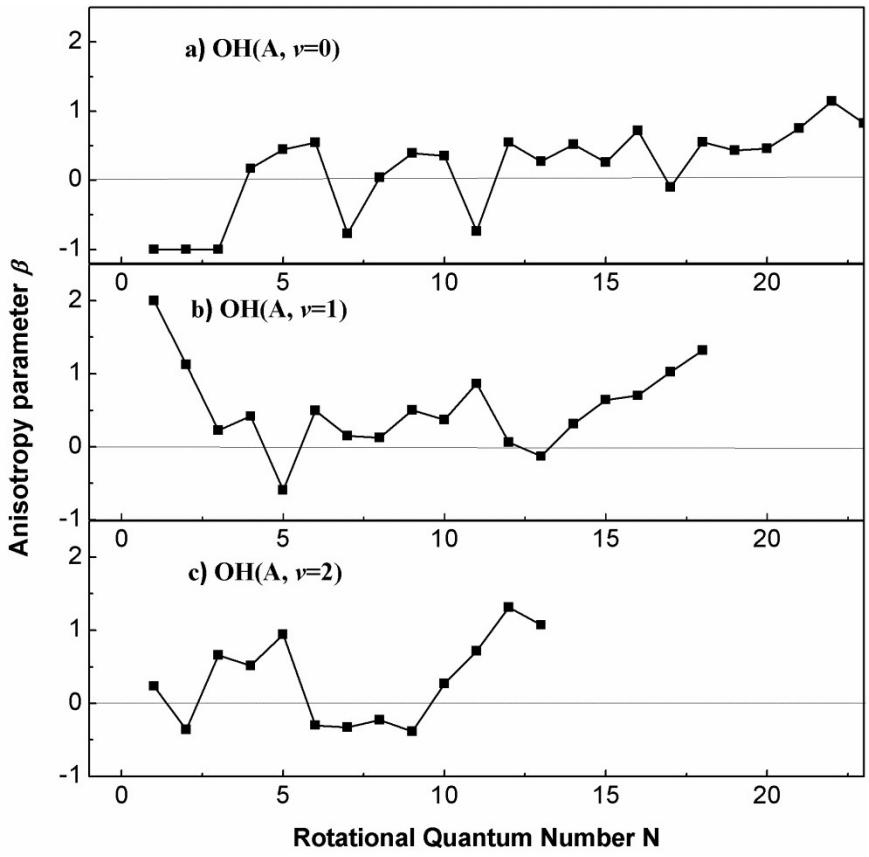

Figure 8. Rotational dependence of the anisotropy parameters for the OH (A, v = 0, 1, 2) products.

View Article Online
DOI: 10.1039/C9CP05321B

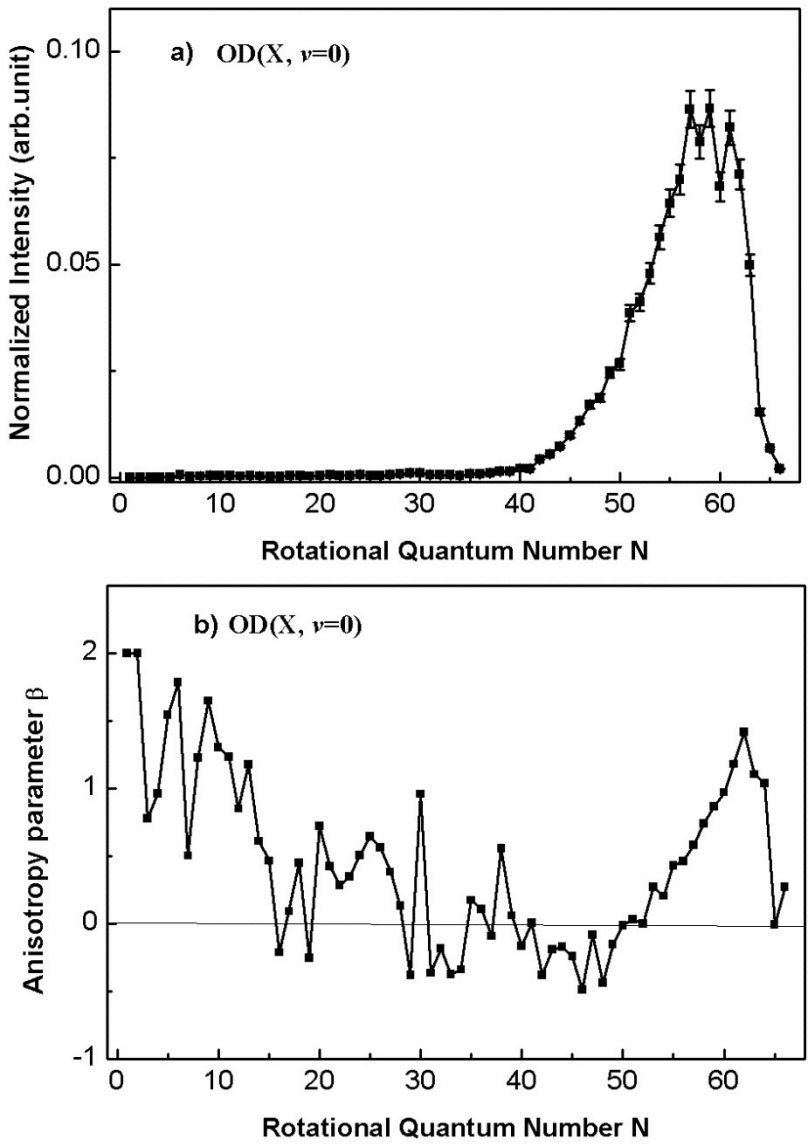

Figure 9. (a) Rotational state distributions of the OD (X, v = 0) products from the photodissociation of D_2O at 121.95 nm and (b) rotational dependence of the anisotropy β for the OD (X, v = 0) products.

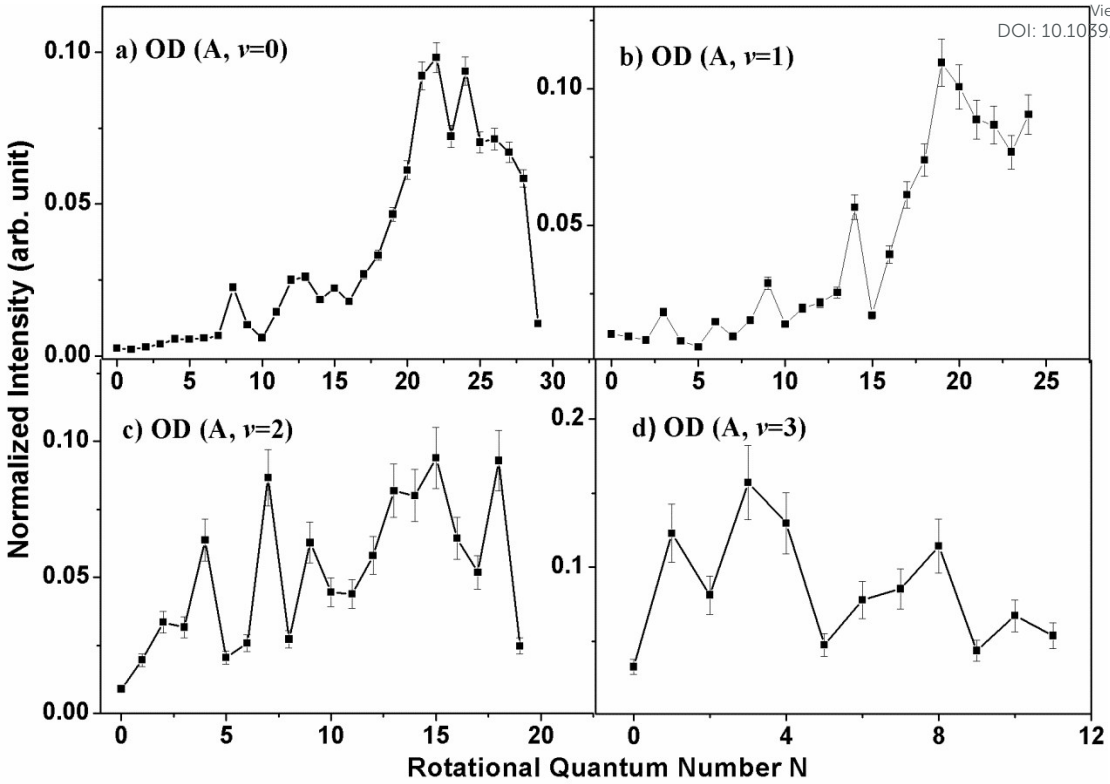

Figure 10. Rotational state distributions of the OD (A, v = 0, 1, 2, 3) products from the photodissociation of D_2O at 121.95 nm.

View Article Online
DOI: 10.1039/C9CP05321B

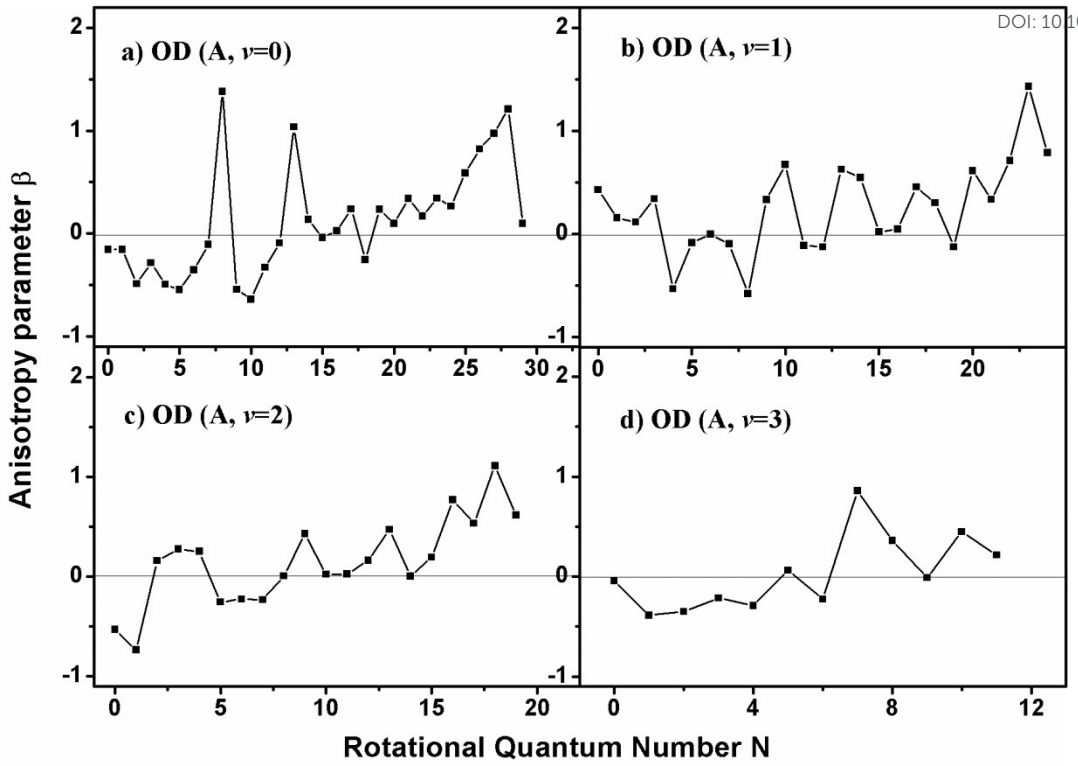

Figure 11. Rotational dependence of the anisotropy parameters for the OD (A, v = 0, 1, 2, 3) products.

View Article Online
DOI: 10.1039/C9CP05321B

Notes and References

1. X. Hu, L. Zhou and D. Xie, *Wires Comput. Mol. Sci.*, 2018, **8**, 1350.
2. X. Yang, *Int. Rev. Phys. Chem.*, 2005, **24**, 37-98.
3. K. J. Yuan, R. N. Dixon and X. M. Yang, *Acc. Chem. Res.*, 2011, **44**, 369-378.
4. R. Mota, R. Parafita, A. Giuliani, M. J. Hubin-Franskin, J. M. C. Lourenço, G. Garcia, S. V. Hoffmann, N. J. Mason, P. A. Ribeiro, M. Raposo and P. Limão-Vieira, *Chem. Phys. Lett.*, 2005, **416**, 152-159.
5. L. Zhou, D. Xie, Z. Sun and H. Guo, *J. Chem. Phys.*, 2014, **140**, 024310.
6. D. W. Hwang, X. Yang and X. Yang, *J. Chem. Phys.*, 1999, **110**, 4119-4122.
7. X. F. Yang, D. W. Hwang, J. J. Lin and X. Ying, *J. Chem. Phys.*, 2000, **113**, 10597.
8. I. C. Lu, F. Wang, K. Yuan, Y. Cheng and X. Yang, *J. Chem. Phys.*, 2008, **128**, 066101.
9. D. Häusler, P. Andresen and R. Schinke, *J. Chem. Phys.*, 1987, **87**, 3949-3965.
10. H. Guo and J. N. Murrell, *Mol. Phys.*, 1988, **65**, 821-827.
11. V. S. B. Yinghua Wu, *J. Phys. Chem. B*, 2002, **106**, 8271-8277.
12. H. Guo and J. N. Murrell, *J. Chem. Soc., Faraday Trans. 2*, 1988, **84**, 949-959.
13. P. Andresen, G. S. Ondrey and B. Titze, *Phys. Rev. Lett.*, 1983, **50**, 486-488.
14. K. Weide and R. Schinke, *J. Chem. Phys.*, 1987, **87**, 4627-4633.
15. L. S. H. J. Krautwald, K. H. Welge, M. N. Ashfold, *Faraday Discuss. Chem. SOC.*, 1986, **82**, 99-110.
16. K. K. B. Heumann, R. Düren, B. Hess, U. Meier, S. D. Peyerimhoff and R. Schinke, *Chem. Phys. Lett.*, 1990, **166**, 385-390.
17. R. v. H. J. H. Fillion, Ruiz, M. Castillejo, A. H. Zanganeh, J. L. Lemaire, M. C. van Hemert, F. Rostas, *J. Phys. Chem. A*, 2001, **105**, 11414-11424.
18. Y. Cheng, K. Yuan, L. Cheng, Q. Guo, D. Dai and X. Yang, *J. Chem. Phys.*, 2011, **134**, 064301.
19. B. H. Michael von Dirke, Klaus Kühl, Thomas Schröder, Reinhard Schinke, *J.*

View Article Online
DOI: 10.1039/C9CP05321B

Chem. Phys., 1994, **101**.

20. L. Zhou, B. Jiang, D. Xie and H. Guo, *J. Phys. Chem. A*, 2013, **117**, 6940-6947.
21. L. Zhou, G. S. M. Lin and D. Xie, *J. Chem. Phys.*, 2013, **139**, 114303.
22. B. Jiang, D. Xie and H. Guo, *J. Chem. Phys.*, 2012, **136**, 034302.
23. S. Su, H. Wang, Z. Chen, S. Yu, D. Dai, K. Yuan and X. Yang, *J. Chem. Phys.*, 2015, **143**, 184302.
24. A. H. Zanganeh, J. H. Fillion, J. Ruiz, M. Castillejo, J. L. Lemaire, N. Shafizadeh and F. Rostas, *J. Chem. Phys.*, 2000, **112**, 5660-5671.
25. R. van Harrevelt and M. C. van Hemert, *J. Chem. Phys.*, 2000, **112**, 5777-5786.
26. R. van Harrevelt and M. C. van Hemert, *J. Chem. Phys.*, 2000, **112**, 5787-5808.
27. S. A. Harich, D. W. H. Hwang, X. Yang, J. J. Lin, X. Yang and R. N. Dixon, *J. Chem. Phys.*, 2000, **113**, 10073-10090.
28. S. A. Harich, X. F. Yang, X. Yang, R. van Harrevelt and M. C. van Hemert, *Phys. Rev. Lett.*, 2001, **87**, 263001.
29. S. A. Harich, X. Yang, D. W. H. Hwang, J. J. Lin, X. Yang and R. N. Dixon, *J. Chem. Phys.*, 2001, **114**, 7830-7837.
30. S. A. Harich, X. Yang, X. Yang and R. N. Dixon, *Phys. Rev. Lett.*, 2001, **87**, 253201.
31. D. W. Hwang, X. F. Yang, S. Harich, J. J. Lin and X. Yang, *J. Chem. Phys.*, 1999, **110**, 4123-4126.
32. R. N. Dixon, D. W. Hwang, X. F. Yang, S. Harich, J. J. Lin and X. Yang, *Science*, 1999, **285**, 1249-1253.
33. D. H. Mordaunt, M. N. R. Ashfold and R. N. Dixon, *J. Chem. Phys.*, 1994, **100**, 7360-7375.
34. W. Yi, J. Park and J. Lee, *Chem. Phys. Lett.*, 2007, **439**, 46-49.
35. J. P. S. A. Hodgson, M. N. Ashfold, J. M. Bayley and R. N. Dixon, *Chem. Phys. Lett.*, 1984, **107**, 1-5.

36. M. N. R. Ashfold, J. M. Bayley and R. N. Dixon, *Can. J. Phys.*, 1984, **62**, 1806-1833.

37. H.-H. Kuge and K. Kleinermanns, *J. Chem. Phys.*, 1989, **90**, 46-52.

38. M.N.R. Ashfold, J.M. Bayley and R. N. Dixon, *Chem. Phys.*, 1984, **84**, 35-50.

39. C. H. Yang, G. Sarma, J. J. Ter Meulen, D. H. Parker and C. M. Western, *Phys. Chem. Chem. Phys.*, 2010, **12**, 13983-13991.

40. K. Yuan, Y. Cheng, L. Cheng, Q. Guo, D. Dai, X. Wang, X. Yang and R. N. Dixon, *Proc. Natl. Acad. Sci. U.S.A*, 2008, **105** 19148–19153.

41. Z. He, D. Yang, Z. Chen, K. Yuan, D. Dai, G. Wu and X. Yang, *Phys. Chem. Chem. Phys.*, 2017, **19**, 29795-29800.

42. Y. Cheng, L. Cheng, Q. Guo, K. Yuan, D. Dai, X. Wang, R. N. Dixon and X. Yang, *J. Chem. Phys.*, 2010, **133**, 034307.

43. R. N. Dixon, T. A. Oliver, L. Cheng, Y. Cheng, K. Yuan and X. Yang, *J. Chem. Phys.*, 2013, **138**, 104306.

44. L. Cheng, K. Yuan, Y. Cheng, Q. Guo, T. Wang, D. Dai, X. Yang and R. N. Dixon, *J. Phys. Chem. A*, 2011, **115**, 1500-1507.

45. Y. Chang, Z. Chen, J. Zhou, Z. Luo, Z. He, G. Wu, M. N. R. Ashfold, K. Yuan and X. Yang, *J. Phys. Chem. Lett.*, 2019, **10**, 4209-4214.

46. K. Yuan, L. Cheng, Y. Cheng, Q. Guo, D. Dai and X. Yang, *J. Chem. Phys.*, 2009, **131**, 074301.

47. D. Hirst and M. Child, *Mol. Phys.*, 1992, **77**, 463-476.

48. O. Steinkellner, F. Noack, H. H. Ritze, W. Radloff and I. V. Hertel, *J. Chem. Phys.*, 2004, **121**, 1765-1770.

49. K. Yuan, L. Cheng, Y. Cheng, Q. Guo, D. Dai and X. Yang, *Rev. Sci. Instrum.*, 2008, **79**, 124101.

50. Y. Chang, S. Yu, Q. Li, Y. Yu, H. Wang, S. Su, Z. Chen, L. Che, X. Wang, W. Zhang, D. Dai, G. Wu, K. Yuan and X. Yang, *Rev. Sci. Instrum.*, 2018, **89**, 063113.

51. S. Su, Y. Dorenkamp, S. Yu, A. M. Wodtke, D. Dai, K. Yuan and X. Yang, *Phys. Chem. Chem. Phys.*, 2016, **18**, 15399-15405.

52. Y. Chang, Y. Yu, H. Wang, X. Hu, Q. Li, J. Yang, S. Su, Z. He, Z. Chen, L. Che, X. Wang, W. Zhang, G. Wu, D. Xie, M. N. R. Ashfold, K. Yuan and X. Yang, *Nat. Commun.*, 2019, **10**, 1250.

53. M. N. R. Ashfold, K. Yuan and X. Yang, *J. Chem. Phys.*, 2018, **149**, 080901.

54. J. P. Marangos, N. Shen, H. Ma, M. H. R. Hutchinson and J. P. Connerade, *J. Opt. Soc. Am. B*, 1990, **7**, 1254-1259.

Contents entry:

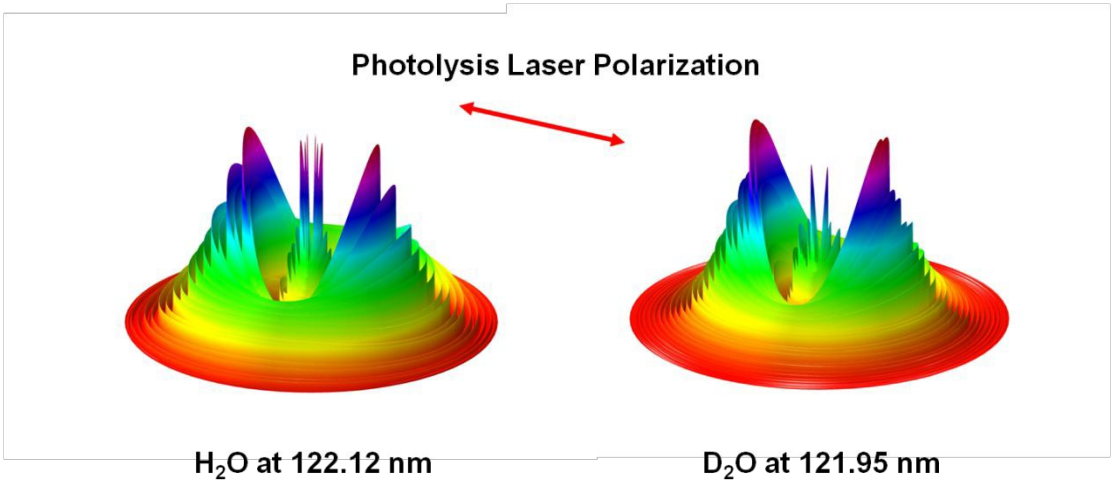

We report the state-to-state dynamical features of H_2O at 122.12 nm and D_2O at 121.95 nm photolysis, which excite to the electronically excited $\tilde{D}$ state.